

CONDENSATION AND SUBSEQUENT ICING ON STRUCTURED PLATE AND GLASS SURFACES IN LOW SPEED FLOWS – AN EXPERIMENTAL STUDY

Christoph Reichl^{1*}, Gernot J. Pauschenwein¹, Bernd Windholz¹, Christoph Zauner¹, Babette Hebenstreit¹, Mustapha Chouiki², Rainer Schöftner² and Michael Monsberger¹

¹ Austrian Institute of Technology, Energy Department, Giefinggasse 3, A-1210 Wien, Österreich

² Profactor GmbH, Functional Surfaces and Nanostructures, Im Statgut A2, 4407 Steyr-Gleink, Austria

* Corresponding Author, christoph.reichl@ait.ac.at

Abstract

Condensation and subsequent icing are critical phase change processes occurring in solar thermal collector physics. Droplets and ice can have a significant impact on solar yield and dropping liquids can lead to a considerable deterioration of coated metal sheets often found in those devices. Therefore it is of utmost importance to understand condensation and the onset of icing and its dependence on relative humidity, flow speed, turbulent structures in the flow and both the surrounding and the plate temperature. In this contribution we focus on the promising application of microstructures in the effected regions of the collector and the utilization of different glass surfaces. The condensation and icing processes in driven turbulent flows on plates and glasses exhibiting varying contact angles due to different surface structures are monitored using high speed and thermo camera visualization techniques. The results will add to the understanding of condensation and icing processes on micro structured plates and glasses and provide the basis for numerical simulations, which will be capable of predicting onset-times, film- and ice-thickness estimations leading to energy efficient and cost-effective designs.

1. Introduction

In [4] an experimental facility to investigate icing and condensation in low speed flows using thermographic and image capturing methods was presented. The facility was characterized with respect to local thermodynamic and flow properties using various experimental techniques including CTA, 3D-PIV, surface temperature sensors and heat sphere probes. The experimental setup and the most important results are summarized in the first part. We will include results from thermocouple and pt100 difference measurements. Then we will present a computational analysis method to gain insight into the data of the image capturing during the underlying phase change processes. This methodology is finally applied to plates and glasses exhibiting different surface structures.

To investigate condensation and icing on micro structured plates (frosting and defrosting of flat plates see e.g. [1]-[3], [5]-[9]) an experimental test rig has been assembled, which consists of a wind tunnel driven by electronically controlled fans and a cooling circuit connected to a stainless steel support plate (see Fig 1). The support plate temperature can be adjusted in a range of -30° C to +80° C. The whole test rig is placed in a climatic chamber, which is capable of providing predefined and stable values of temperature and relative humidity. The phase change processes are monitored using "high-speed" and thermo camera visualization techniques.

2. Experimental Setup

The experimental setup used for the phase change studies consists of a wind tunnel driven by fans. The temperature of the test section plate is controlled via an external heat exchanger unit (see Fig 1). The wind tunnel was constructed mainly using stainless steel and aluminium parts. The test section is covered using an acrylic-glass part, which provides 3-side optical access. The cross section of the wind tunnel is 300 mm x 100 mm. The different flow fields are generated using three axial fans. They can be drive controlled using pulse width modulation providing a maximum volume flow of 500 m³/h each (see Fig 1 left). An ultra-low-refrigerated circulator using the refrigerant R507 was used to keep the test section plate attached to the heat exchanger at constant temperature. The temperature control liquid is capable of stabilizing the temperature in a range of -30° C to +80° C. The cooling capacity of the heat exchanger unit is not constant with temperature (2000 W at +20° C down to 260 W at -40° C), while the heater capacity is 3000 W independent of the fluid temperature. The pump was set to its maximum, producing flow rates around 22 l/min. The heat exchanger circuit is stabilized in a range of $\pm 0.05^\circ$ C using self-optimized intelligent cascade controlling.

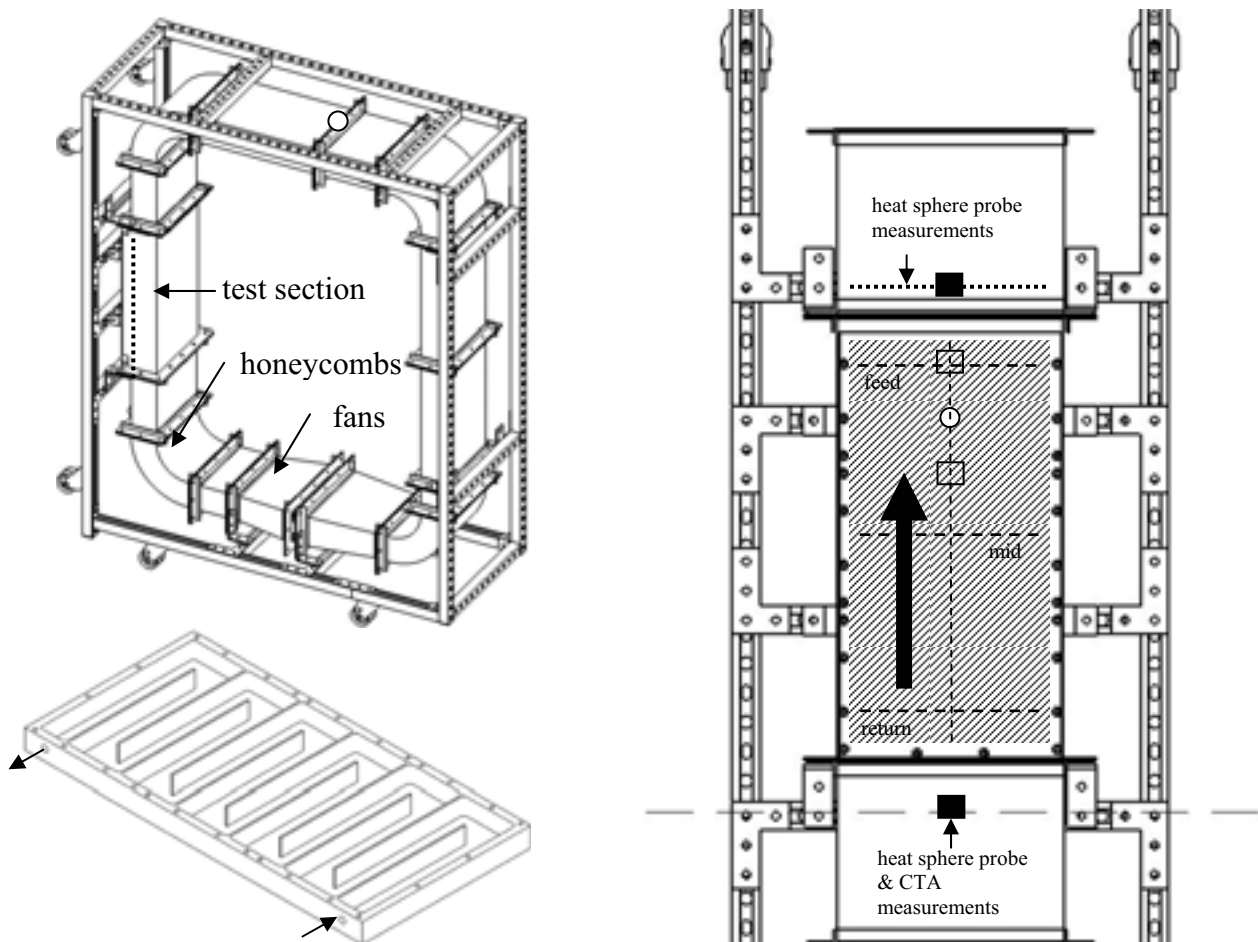


Fig 1. Experimental Setup. Upper left: inclined crack of the full closed channel setup. The dotted line marks the position of the heat exchanger unit. Lower left: heat exchanger unit (cover removed). The arrows show the fluid flow direction. Right: front view of the test section (hatched area surrounded by mounting holes), where the humid air enters from the bottom and leaves at the top. The dashed line marks the position of the CTA measurements. Additional point probe air velocity measurements have been performed at points on the long dashed and dotted line. The large black arrow shows the flow direction. Positions for the thermocouple pair are marked with a open square, pt100 positions for difference measurements are marked with a solid square (see also [4]).

3. Measurement & Analysis Techniques

Several measurement techniques have already been applied [4] to assess the temperature, flow and humidity conditions of the setup. Surface temperature and humidity sensors, heat sphere probes, CTA, PIV, thermography and image capturing techniques have been used.

The test section surface temperature was scanned along horizontal and vertical lines using a fast reacting surface temperature probe with elastic thermo couple bands. For humidity and temperature measurements of the air flow downstream of the fans a standard room climate sensor was used. The velocity measurements have been performed using a heat sphere probe. The CTA scanning was based on a 3D traversing mechanism fully controlled by the acquisition computer. The CTA data was acquired using a 16 Bit 250 kS/s. Flow homogeneity tests have been performed using a 3D PIV consisting of one high speed camera and one camera using framegrabber technology. Both cameras were equipped with a 60mm lens. An infrared heat image system was used for capturing the surface temperature of the aluminium test section plate. Image capturing was performed with a DV video camera equipped with a 120x objective using fixed white balance correction and manual focus. Promising results could be reached using a setup of six lamps using a blue LED with a luminosity of 50 cd producing a radiation angle of 12° by only introducing a total of 4.8 W power. Image acquisition was realized via the fire wire port direct link.

Water contact angle measurements for glasses exhibiting different surfaces were made using distilled water and a Krüss DSA 100 goniometer (see Table 2).

The UV-Vis transmission spectra of the prepared glass samples were recorded on a Perkin Elmer Lambda 35 UV-Vis spectrophotometer in the 190-900 nm wavelengths range with a 1 nm resolution (see Fig. 7).

For an automated analysis of the video data the amount of available information from the videos has to be reduced. This was performed in the following steps: Firstly, one frame per second proved sufficient to cover the relevant processes. Secondly, the RGB values of each pixel are translated into the according HSL (hue, saturation, lightness) values and only the L value is kept. This has also been done for the difference images/frames, where the difference between each considered frame and an initial reference frame is computed. Thirdly, the average lightness (0=black, 1=white) of all pixels contained in one region/tile is calculated and plotted against time (see fig. 3 as an example). From the lightness curves of the difference frames one can also automatically retrieve the starting time of condensation. Initially the difference-lightness attains of course a value close to 0, and when the condensation starts it rises very sharply. If one fits a continuous function which is constant for $t < t_c$ and linear above to the data until shortly after the sharp rise, one obtains the estimated condensation time t_c with an error bar resulting from the noise-range. To obtain a similar procedure for the icing process there is still more effort necessary, since the lightness or difference-lightness curves can behave very differently for the various considered surfaces.

4. Thermodynamic and Flow Characterization

Application of the introduced experimental techniques yield the following results: The vertical temperature gradient is 0.2° C, the horizontal temperature gradients depend on the position and ranges from 0.6° C in the 'feed' line to 0.2° C in the 'return' line (see Fig 1). The surface temperature follows the heat exchanger fluid temperature nicely with an offset of around +2.8° C at -20° C. Combining the information of the heat sphere probes, the CTA measurements and the 3D PIV analysis, the establishing flow patterns in the wind tunnel are given to be slightly asymmetric with higher values on one wind tunnel side. This effect, however, is only effective at higher fan power settings. For a typical fan power of 40%, the flow is homogeneous with a mean velocity of 2.3 m/s.

5. Experimental Results for the Stainless Steel Heat Exchanger Backplate

A thermocouple pair was positioned in the upper third of the measurement zone (open squares in Fig 1). Two pt100 RTDs (resistor temperature dependent) have been placed up- and downstream of the measurement zone (see solid squares in Fig. 1)

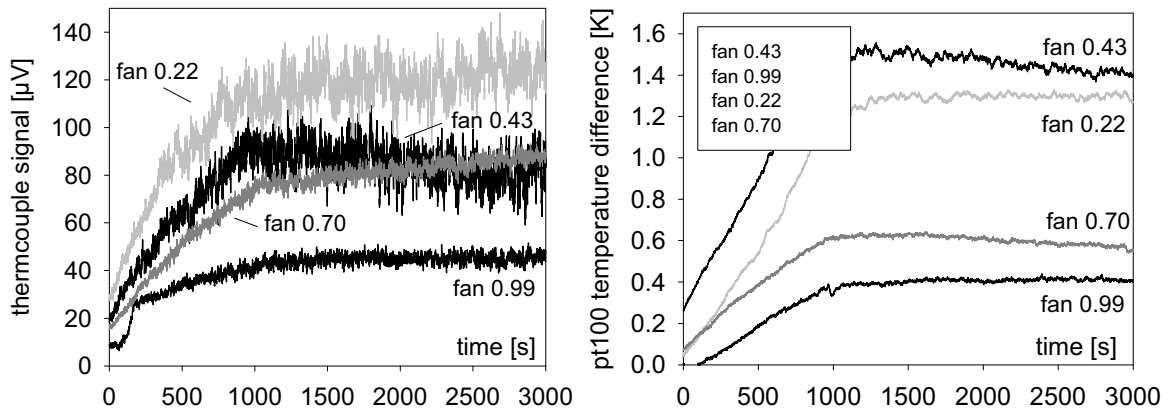


Fig. 2. thermocouple signal (left) and pt100 temperature difference (right) as a function of time for different flow speeds (ranging between 1 m/s and 8 m/s). The flow temperature was kept fix at 24° C, the rel. humidity was 37%.

Reducing the flow speed (see Fig. 2 left) significantly, the thermocouple signals increases. Higher flow velocities lead to smaller values of the thermocouple signal. The incoming air cannot be cooled to a large extent. A similar picture can be gained by using two pt100 RTDs. The upper two curves, however, change position in comparison to the thermocouple pair.

Measurements changing the relative humidity while keeping flow speed (2 m/s) and temperature (22°C) constant have already been discussed in [4]. Computational image processing now allows for a more quantitative analysis (see Fig. 3).

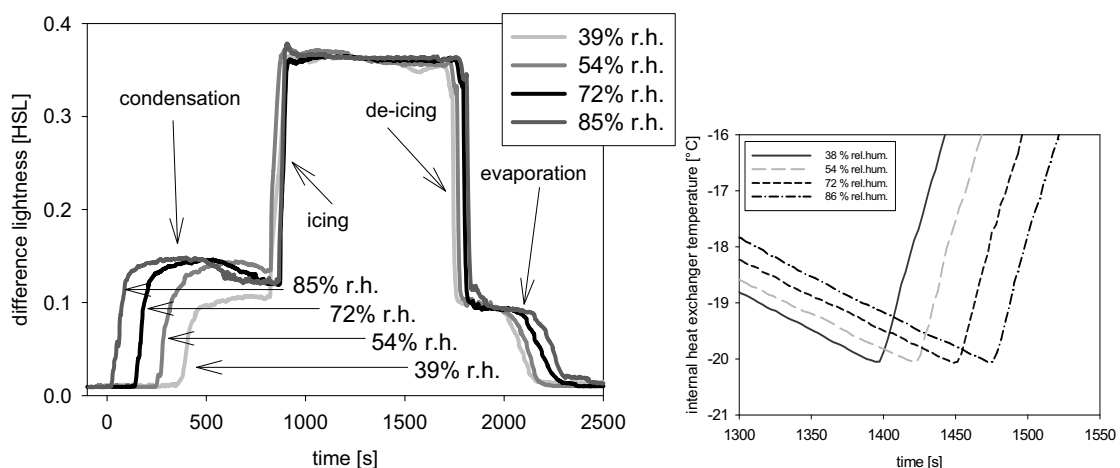


Fig. 3. Difference lightness [HSL] signal of the condensation, icing, de-icing and evaporation processes (left) with varying rel. humidity, flow temperature ~22° C, flow speed 2 m/s. The cooling curves of the heat exchanger fluid are showing the setpoint change times (right, [4]).

Depending on the humidity (flow speed and temperature is fixed) condensation occurs separated in time. Icing and de-icing, however, can be extracted as a sharper process only separated by times in the range of 1-2 minutes. Evaporation occurs in reverse order to the condensation process.

6. Experimental Results for Structured Plates

In addition to a flat plate, three different micro structures have been selected (see Table 1). The wind tunnel setup was tilted to an angle of approx. 40° .

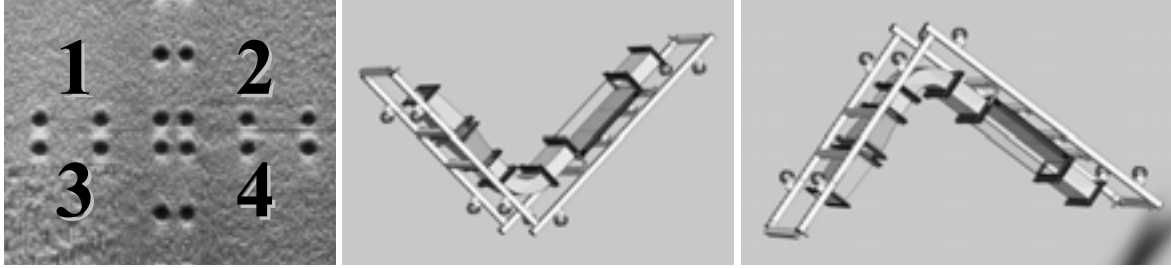


Fig 4. Plate numbering (left), tilted setup for structured plates (mid) and inverse setup for drop tests from glasses (right, see Fig. 10)

Table 1. Definition of structured plates

plate 1	flat plate, no structure	plate 2	halfpipes with diameter 0.5 mm
plate 3	halfpipes with diameter 1 mm	plate 4	triangle with round bottom

Fig. 5 shows the difference lightness revealing condensation and subsequent icing processes of the 4 different plates. The heat exchanger temperature was driven down to -30° . De-icing and de-fogging was reached by subsequently increasing the temperature to $+50^\circ$ (see dashed lines in Fig. 5).

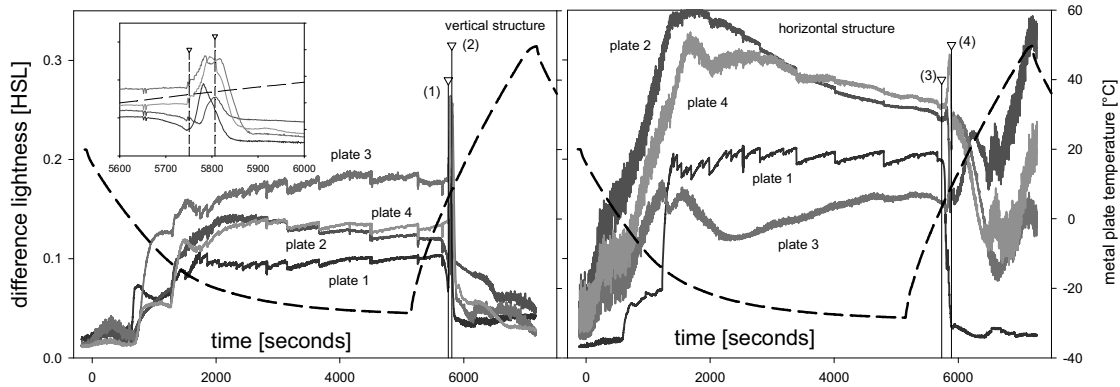


Fig. 5. Difference lightness [HSL] signal of the phase change process on structured plates (left = vertical, right = horizontal structures). The dashed line shows the heat exchanger temperature (right scale). Rel. humidity $\sim 60\%$, flow temperature $\sim 12^\circ\text{C}$, flow speed 2 m/s. (left: vertical structures, right: horizontal structures). Triangles with droplines correspond to the snapshots in fig 6. A detailed view of full ice and de-fogging of the left figure is given in its insert.

The horizontally structured plates show larger noise, which can be attributed to the stronger reflectivity of these plates for the chosen light position. Vibrations of the plates due to the fans lead to increased levels of scattered light in this case. Significant shifts in icing times can be seen for the vertically structured plates separating for example plate 3 and plate 4 by approximately 300 seconds. It can be seen, that reflectivity changes in steps as ice is formed and ice growth takes place. The signal increase for the horizontal plates at 6500 seconds can be attributed to remaining water droplets and water structures on the plate (see also Fig. 6). This effect can not be seen for the vertical plates, as water can run down the microstructure.

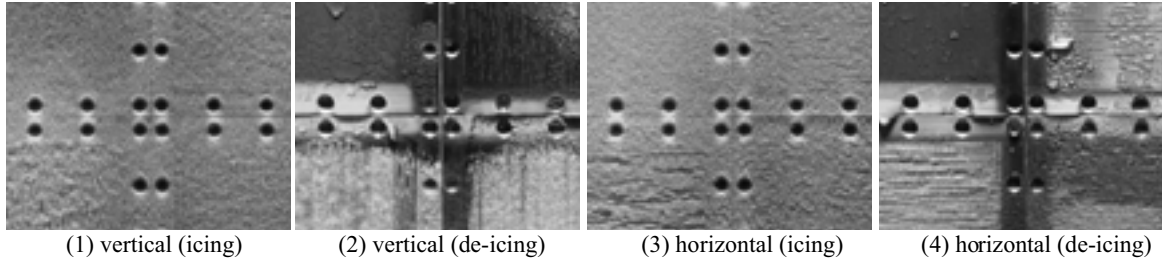


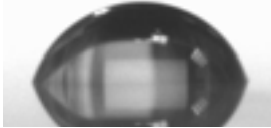







Fig. 6. Icing and de-icing of vertical and horizontal structured plates. All four structures have been placed simultaneously on the backplate. First row = plate 1 (left) and plate 2 (right), second row plate 3 (left) and plate 4 (right).

7. Experimental Results for Glasses with different surface structures

Table 2 introduces eight structured glass plates. The contact angle can be extracted from the graphical representation and ranges from 10° to 118° . The untreated glass plate (reference) has a contact angle of 20° .

Table 2. glass structure specifications and contact angle with water of different glass specimens

name (contact angle with water)	contact angle measurement	name (contact angle with water)	contact angle measurement
{1} reference ($\theta = 20^\circ$)		{5} M5C6F3 ($\theta = 100^\circ$)	
{2} HMDS ($\theta = 70^\circ$)		{6} MSL ($\theta = 102^\circ$)	
{3} MC6 ($\theta = 87^\circ$)		{7} SiH ($\theta = 106^\circ$)	
{4} self-cleaning (Ti O ₂) ($\theta = 10^\circ$)		{8} nanostructured ($\theta = 118^\circ$)	

The transmission spectra of the samples are shown in Fig. 7. A high transparency (91-93%) is observed above 350 nm for most of the samples. The small variation in the transmission signal {1}, {2}, {3}, {5}, {6}, {7} is due to the glass itself. For self-cleaning and nanostructured glasses who absorb in the visible region, the transmission is not high enough to be used in solar thermal applications.

Cooling the heat exchanger plate down to -5° , condensation and subsequent icing can be seen on the different glass structures (see Fig. 8). By stopping the cooling process at 0°C for a time span of approx. 1700 seconds and then increasing the temperature to $+40^\circ\text{C}$, condensation and evaporation can be studied (see Fig. 9 left).

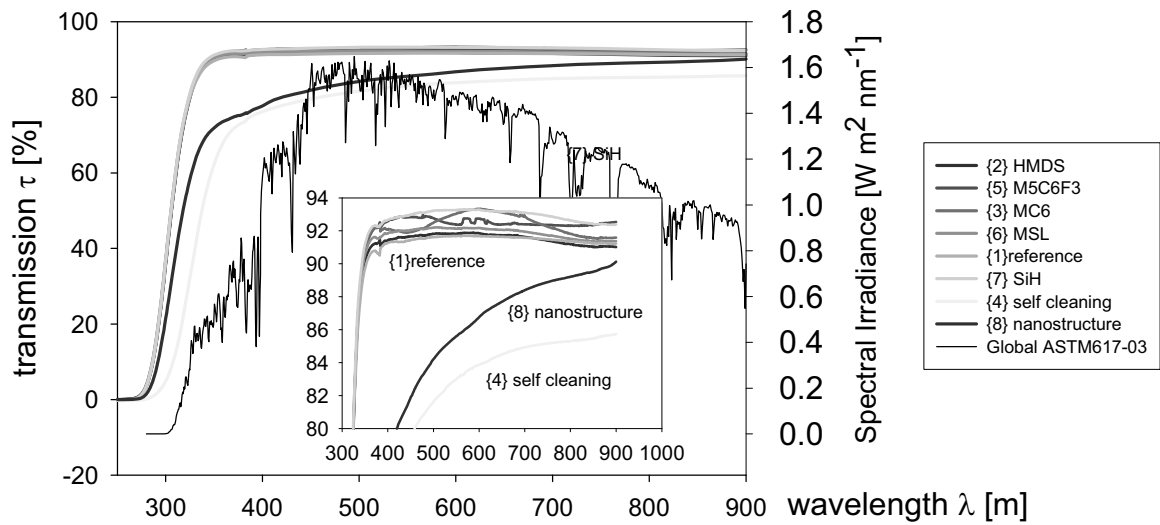


Fig. 7. UV-Vis spectroscopy transmission spectra of the glass samples - the insert shows a magnification of the 80-94 % transmission range. The global spectral irradiance is added (right scale).

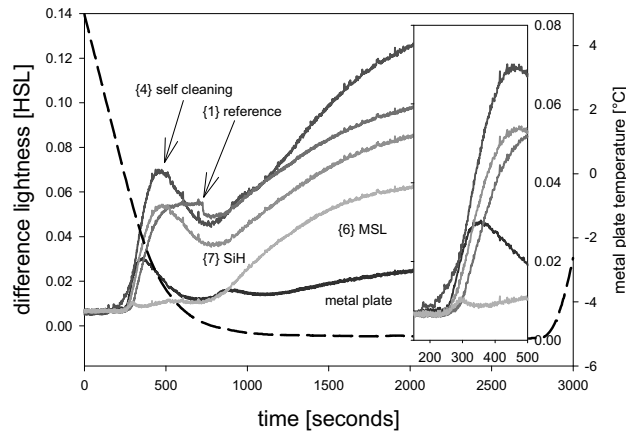


Fig. 8. Difference lightness [HSL] signal of the condensation process on differently treated glass plates. The dashed line shows the heat exchanger temperature (right scale). rel. humidity $\sim 71\%$, flow temperature $\sim 5^\circ\text{C}$, flow speed 1 m/s.

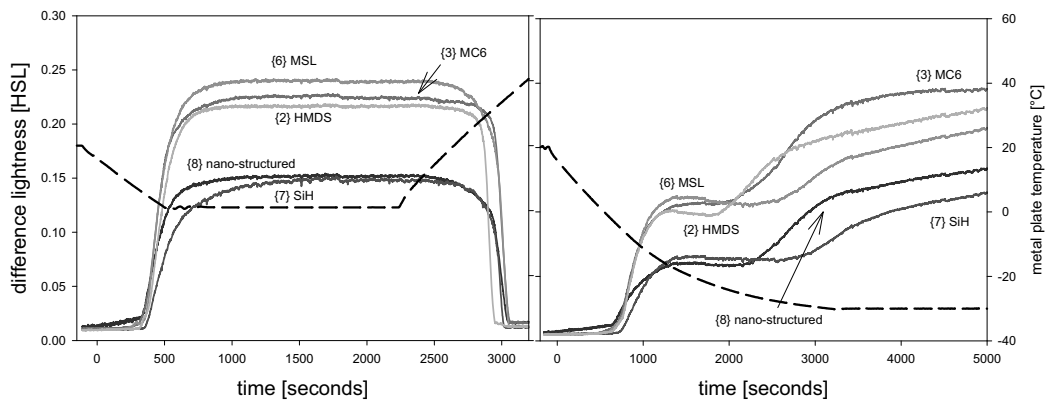


Fig. 9. Difference lightness [HSL] signal of the condensation process on differently treated glass plates. The dashed line shows the heat exchanger temperature (right scale). (left) rel. humidity $\sim 78\%$, flow temperature $\sim 12^\circ\text{C}$, flow speed 1 m/s, (right) rel. humidity $\sim 68\%$, flow temperature $\sim 6^\circ\text{C}$, flow speed 1 m/s.

The differences in the condensation and de-fogging times can be extracted from Fig. 9. However, small errors due to variations in the backplate temperature (see section 4) and not evenly distributed heat conductive paste have to be considered. Icing processes (see Fig 9 right) seem to occur at significantly shifted times.

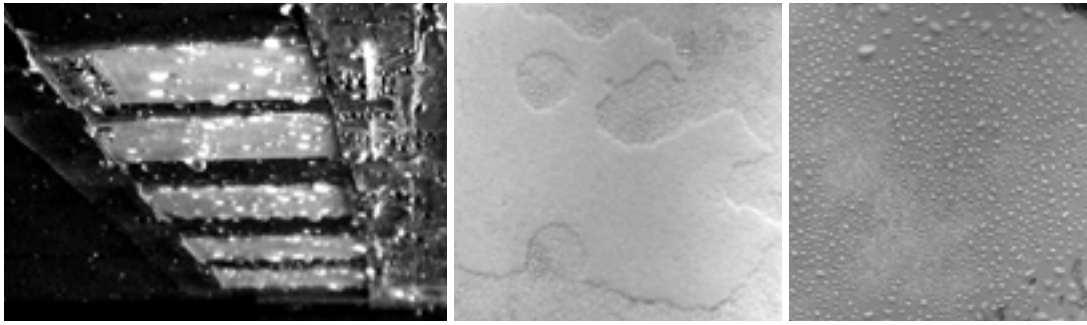


Fig. 10. During de-icing on an inverse tilted setup (see Fig. 4 right) drops are forming on the glass surfaces (left) – Water film and water droplets on glass surfaces (mid & right).

8. Conclusion & Outlook

We presented a setup for studying phase-change processes on cooled plate surfaces, structured metal and glass surfaces. Measurements have been performed at different flow temperatures and different values of the relative humidity by placing the experimental test rig in a climatic chamber. A computational image analysis was presented and successfully applied to the available data. Metal plates with different microstructures show diverse icing and de-icing patterns and times. Horizontally mounted, an increase in reflectivity due to remaining water droplets and water structures could be observed. Phase change processes on structured glass surfaces with different contact angles and UV transmissivity have shown, that condensation and evaporation occur in a smaller time range compared to the various ice formation stages, which are more separated. To further investigate the behaviour of structured glasses, a significant increase in surface area seems to be necessary to avoid possible boundary effects. In addition to hydrophobic glass surfaces studies of more hydrophilic ones will be performed. The proposed methodology seems to be a promising option for accessing phase change occurrence and duration process times for comparison of different surface structures of metals and glasses. This data will be subsequently used to aid in numerical simulation techniques, which are currently investigated.

References

- [1] N. Aljuwayhel, D. Reindl, S. Klein, G. Nellis (2007), Comparison of parallel- and counter-flow circuiting in an industrial evaporator under frosting conditions, *International Journal of Refrigeration* 30(8), 1347--1357.
- [2] K. Lee, S. Jhee, D. Yang (2003), Prediction of the frost formation on a cold flat surface, *International Journal of Heat and Mass Transfer* 46(20), 3789--3796.
- [3] S. Roy, H. Kumar, R. Anderson, R. (2005), Efficient defrosting of an inclined flat surface, *International Journal of Heat and Mass Transfer* 48(13), 2613--2624.
- [4] Ch. Reichl et al., IIR 1st Conference on Sustainable Refrigeration and Heat Pump Technology, Stockholm, submitted (2010).
- [5] H. Egolf (1984), Grundlagen zur experimentellen Bestimmung der Bereifung von Luftkühlern, Diss. ETH Zürich, Nr. 7509, 1984
- [6] S. A. Tassou, C. J. Marquand (1987), Effects of evaporator frosting and defrosting on the performance of air-to-water heat pumps, *Applied Energy* 28(1), 19--33.
- [7] R. O. Piucco, C. J. Hermes, C. Melo, and J. R. B. Jr., A study of frost nucleation on flat surfaces, *Exp. Therm Fluid Sci* 32, 1710 (2008)
- [8] X. Wu, W. Dai, W. Xu, and L. Tang, Mesoscale investigation of frost formation on a cold surface, *Experimental Thermal and Fluid Science*, 31, 1043 (2007)
- [9] K.-S. Lee, S. Jhee, D.-K. Yang, Prediction of the frost formation on a cold flat surface, *Int. J. Heat Mass Tran.*, 46, 3789 (2003)